

## INTERPRETING THE CLUSTERING OF DISTANT RED GALAXIES

JEREMY L. TINKER<sup>1</sup>, RISA H. WECHSLER<sup>2</sup>, & ZHENG ZHENG<sup>3</sup>

<sup>1</sup> Berkeley Center for Cosmological Physics, University of California-Berkeley; [tinker@berkeley.edu](mailto:tinker@berkeley.edu)

<sup>2</sup> Kavli Institute for Particle Astrophysics and Cosmology, Dept. of Physics, and SLAC National Laboratory, Stanford University

<sup>3</sup> John Bahcall Fellow, School of Natural Sciences, Institute for Advanced Study

*Draft version October 27, 2018*

### ABSTRACT

We analyze the angular clustering of  $z \sim 2.3$  distant red galaxies (DRGs) measured by Quadri et al. (2008). We find that, with robust estimates of the measurement errors and realistic halo occupation distribution modeling, the measured clustering can be well fit within standard halo occupation models, in contrast to previous results. However, in order to fit the strong break in  $w(\theta)$  at  $\theta = 10''$ , nearly all satellite galaxies in the DRG luminosity range are required to be DRGs. Within this luminosity-threshold sample, the fraction of galaxies that are DRGs is  $\sim 44\%$ , implying that the formation of DRGs is more efficient for satellite galaxies than for central galaxies. Despite the evolved stellar populations contained within DRGs at  $z = 2.3$ , 90% of satellite galaxies in the DRG luminosity range have been accreted within 500 Myr. Thus, satellite DRGs must have known they would become satellites well before the time of their accretion. This implies that the formation of DRGs correlates with large-scale environment at fixed halo mass, although the large-scale bias of DRGs can be well fit without such assumptions. Further data are required to resolve this issue. Using the observational estimate that  $\sim 30\%$  of DRGs have no ongoing star formation, we infer a timescale for star formation quenching for satellite galaxies of 450 Myr, although the uncertainty on this number is large. However, unless all non-star forming satellite DRGs were quenched before accretion, the quenching timescale is significantly shorter than  $z \sim 0$  estimates. Down to the completeness limit of the Quadri et al sample, we find that the halo masses of central DRGs are  $\sim 50\%$  higher than non-DRGs in the same luminosity range, but at the highest halo masses the central galaxies are DRGs only  $\sim 2/3$  of the time.

*Subject headings:* cosmology: theory — galaxies:clustering — galaxies: halos — galaxies:formation — large-scale structure of universe

### 1. INTRODUCTION

Distant red galaxies (hereafter DRGs) are bright near-infrared-selected galaxies that have been detected out to  $z \sim 3$  (Franx et al. 2003; van Dokkum et al. 2003; Daddi et al. 2003). These galaxies are massive objects containing a significant population of evolved stars (Förster Schreiber et al. 2004), with many galaxies having highly suppressed star formation or possibly none at all (Labbé et al. 2005; Kriek et al. 2006). Given the remarkable fact that these evolved (and possibly dead) galaxies existed a mere 2 Gyr after the big bang, many studies have further sought to measure their abundance and clustering to determine their connection to dark matter structure (Daddi et al. 2003; Grazian et al. 2006; Quadri et al. 2007, 2008; Marchesini et al. 2007; Ichikawa et al. 2007).

Daddi et al. (2003) measured a very strong clustering strength for DRGs, implying that these galaxies live in only the most massive dark matter halos that exist at such high redshift. In fact, the number density of such halos was significantly smaller than the observed space density of the DRGs themselves. Daddi et al. (2003) used measurements of small-scale clustering to find the correlation length of their sample through extrapolation to larger scales. Using the halo occupation distribution to model the clustering (HOD; see Cooray & Sheth 2002 for a review), Zheng (2004) demonstrated that the high clustering strength and observed number density were compatible by taking into account a small fraction of DRGs that are satellite galaxies orbiting around other DRGs that sit at the center of the dark matter halo. This small satellite fraction produces a significant difference in the slope of the correlation function at large and small scales.

Quadri et al. (2008) (hereafter Q08) used a much larger sample of DRGs to confirm the strong clustering of Daddi et al. (2003) and subsequent studies, both at large ( $\sim 20 h^{-1}$  Mpc) and small ( $\sim 200 h^{-1}$  kpc) scales. They attempted to model the data with a somewhat different HOD approach from Zheng (2004), but they could not find a satisfactory fit: models that fit at small scales underpredicted the large-scale bias, while models that reproduced the large-scale bias overpredicted the small-scale clustering. They proposed that standard assumptions of HOD models do not describe these galaxies; their halo occupation correlates with large-scale environment as well as halo mass, i.e., the so-called “assembly bias” (Croton et al. 2007; Wechsler et al. 2006; Gao & White 2007). This correlation would imply that galaxy formation depends on large-scale environment at fixed halo mass, a correlation not seen in low-redshift data (Tinker et al. 2008b).

In this paper we demonstrate that the observations of Q08 can be well-fit by standard HOD models. The inclusion of cosmic variance in the large-scale clustering errors ameliorates much of the discrepancy with their model fits. We also show that a more physically motivated halo occupation model yields significantly better results in fitting the data as well. Further, we will use our HOD modeling to test the mechanisms for the formation of red galaxies at  $z > 2$ .

Unless otherwise stated, all calculations adopt a flat  $\Lambda$ CDM cosmology consistent with the latest constraints from CMB anisotropies (Dunkley et al. 2008). Our cosmological parameter set is  $(\Omega_m, \sigma_8, h, n_s, \Omega_b) = (0.25, 0.8, 0.7, 0.95, 0.045)$ . All distances are comoving. Due to their color selection, throughout this paper we will use the terms DRGs and “red galaxies” interchangeably.

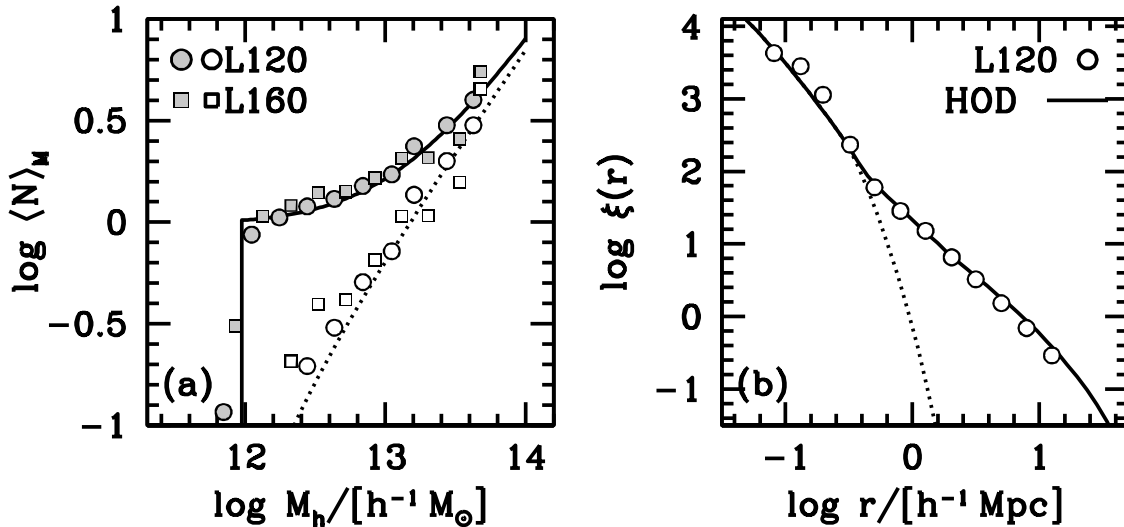


FIG. 1.— Panel (a): Halo occupation functions produced by the abundance matching method described in the text. Gray symbols represent all halos (parent+sub) while white symbols represent only the subhalos. The two simulations have two different cosmologies, so they have been shifted to a common mass scale to demonstrate self-similarity. The solid and dotted curves represent the HOD used in all analytic calculations henceforth. Panel (b): Comparison between the clustering in the L120 box and the analytic model. The HOD for the analytic model is obtained from fitting the simulation results (e.g., panel a, but shifted to the proper mass scale). The solid line is the full correlation function, and the dotted line the one-halo term.

## 2. METHODS

### 2.1. Definition of the Term “Halo”

Because we will be dealing with halos that exist in various environments, it is important to have a clear definition of a halo and discuss what it implies. We assume that all galaxies live at the center of a virialized clump of dark matter. That dark matter clump may be isolated or it may exist within the virial radius of a larger structure. Therefore we will use the term *halo* to refer to an object that is distinct; i.e., it does not exist within the virial radius of another object. These objects typically have a mean overdensity of  $\sim 200$  times that of the background universe. We refer to objects inside the virial radius of halos as *subhalos*. We use the term *galactic halos* to refer to all halos, both halos and subhalos, that contain galaxies at their center.

### 2.2. Halo Occupation from Simulations

Although collisionless  $N$ -body simulations do not include any baryon physics, one can associate the likely sites of galaxy formation with the dark matter halos and subhalos within a simulation. Several recent studies have demonstrated the robustness of this assumption by comparing the clustering of galaxies to that of a sample of galactic halos with the same space density; i.e., galaxies brighter than a given luminosity threshold compared with galactic halos more massive than a threshold that yields the same abundance. Conroy et al. (2006) found that the predicted galactic halo clustering was consistent with galaxy two-point clustering measurements from  $z = 0$  to  $z = 5$  (see also Kravtsov et al. 2004; Wang et al. 2006). Marín et al. (2008) extended this to measurements of the galaxy three-point correlation function as well.

For the purpose of this paper, we use high-resolution cosmological  $N$ -body simulations to guide our choice of the halo occupation of all galaxies (DRGs and non-DRGs). The HOD for all galaxies is then fixed by making use of the luminosity function of all galaxies (see below), and we focus our effort

TABLE 1  
LIST OF SIMULATIONS

$L_{\text{box}} (h^{-1} \text{Mpc})$	$(\Omega_m, \sigma_8, n_s)$	$m_p [h^{-1} M_\odot]$	$z_{\text{out}}$
120	(0.3, 0.9, 1.0)	$1.07 \times 10^9$	2.0
160	(0.24, 0.75, 0.95)	$2.54 \times 10^8$	2.5
1000	(0.27, 0.8, 0.95)	$6.98 \times 10^{10}$	2.5

NOTE. — Each simulation will be referred to in the text by its box size. All simulations were performed with the ART code of Kravtsov et al. (1997). The L120 and L1000 simulations have been described in Tinker et al. (2008a).

on constraining the DRG HOD from the clustering data.

Just knowing where the galaxies are, however, doesn’t identify which ones are red. Before creating a model for the halo occupation of DRGs, we first use the subhalo abundance matching technique (SHAM) to set the occupation of *all* galaxies down to the completeness limit of Q08. The space density of DRGs in the Q08 sample is  $\bar{n}_{\text{DRG}} = 6.5 \times 10^{-4} (h^{-1} \text{Mpc})^{-3}$  down to their completeness limit of  $K < 21$ . Using the  $z \sim 2.3$  luminosity function of Marchesini et al. (2007), the space density of all galaxies is  $1.5 \times 10^{-3} (h^{-1} \text{Mpc})^{-3}$  at the same magnitude threshold,  $M_R = -22.3$ , yielding a DRG fraction of 44%.<sup>1</sup> Whenever referring to the sample of *all galaxies*, we mean all galaxies (DRGs and non-DRGs) down to the completeness limit of the Q08 sample.

Figure 1a shows the halo occupation functions,  $\langle N \rangle_M$ , of

<sup>1</sup> As Q08 point out, the space density of DRGs from Marchesini et al. (2007) is slightly lower than that of the larger Q08 sample. Thus, whenever using the Marchesini et al. (2007) luminosity functions and data, a correction factor of  $6.5/5 \approx 1.3$  is applied. This increases the published number density of galaxies brighter than  $M_R = -22.3$  in Marchesini et al. (2007) from  $1.2 \times 10^{-3}$  to  $1.5 \times 10^{-3} (h^{-1} \text{Mpc})^{-3}$ .

halos and subhalos above a given maximum circular velocity such that the space density of all galaxies down to the Q08 limit is obtained. We use results from the first two simulations listed in Table 1. Halos and subhalos are identified in the simulation by the algorithm described in Kravtsov et al. (2004), a variant of the spherical overdensity halo finder. Because the simulations have different cosmologies and redshifts,  $\langle N \rangle_M$  will differ between the two. However, the *shape* of  $\langle N \rangle_M$  is self-similar. The HOD from both simulations is well approximated by a satellite occupation function of the form

$$\langle N_{\text{sat}} \rangle_M = \left( \frac{M}{M_1} \right)^{\alpha_{\text{sat}}} \exp \left( -\frac{M_{\text{cut}}}{M} \right), \quad (1)$$

where  $\alpha_{\text{sat}} = 1$ , and a central occupation function of the form

$$\langle N_{\text{cen}} \rangle_M = \begin{cases} 1 & \text{if } M \geq M_{\text{min}} \\ 0 & \text{if } M < M_{\text{min}}. \end{cases} \quad (2)$$

Both simulations exhibit the mass ratios  $M_1/M_{\text{min}} = 15.7$  and  $M_{\text{cut}}/M_{\text{min}} = 1.14$ . To match the number density of all galaxies in our fiducial cosmology, a value of  $M_{\text{min}} = 9 \times 10^{11} h^{-1} M_{\odot}$  is required. This yields values of  $M_1 = 1.4 \times 10^{13} h^{-1} M_{\odot}$ , and  $M_{\text{cut}} = 1.0 \times 10^{12} h^{-1} M_{\odot}$ . In Figure 1a, the HOD from L120, a simulation with WMAP1 cosmological parameters (Spergel et al. 2003), has been shifted by  $-0.25$  dex in halo mass. The results from L160, a simulation closer to the WMAP3 cosmological parameter set (Spergel et al. 2007), have been shifted by  $+0.23$  dex. These shifts bring the HODs into alignment with the HOD for our fiducial cosmology. In the L120 box at  $z = 2$ , the total fraction of galactic halos that are subhalos is 13%. This is in good agreement with Conroy et al. (2006) but somewhat smaller than the subhalo fraction of Wetzel et al. (2008), who find 18%. This is most likely attributable to differing classifications of a subhalo. In our definition, a halo becomes a subhalo when it passes the spherical virial radius of a larger halo. In Wetzel et al. (2008), halos become subhalos when they are linked by the friends-of-friends algorithm, which can link objects outside of what we have defined as the virial radius.

With  $\langle N \rangle_M$  specified, we can analytically calculate the galaxy two-point autocorrelation  $\xi(r)$ . Our model for  $\xi(r)$  is based on the analytic model detailed in Zheng (2004) and Tinker et al. (2005). We use a Poisson distribution for the scatter about  $\langle N_{\text{sat}} \rangle_M$ , in agreement with simulations and semi-analytic models (Kravtsov et al. 2004; Zheng et al. 2005) and with observations of galaxy clusters (Kochanek et al. 2003; Lin et al. 2004). We also assume that the satellite galaxies follow the radial distribution of dark matter within the halos (e.g., the density profile of Navarro et al. 1996), using the halo concentrations of Zhao et al. 2008. We use the Tinker et al. (2008a) mass function for  $\Delta = 200$  and a new halo bias function based on those simulations (Tinker et. al., in prep; see Appendix A). Our analytic model incorporates scale-dependent halo bias and halo exclusion for proper modeling of the transition between the one-halo term and the two-halo term. It has been fully tested against numerical simulations (Zehavi et al. 2004; Tinker et al. 2005; Chen 2007; Wechsler et. al. 2009, in preparation).

The clustering statistic measured by Q08 is the angular correlation function  $w(\theta)$ . The three-dimensional correlation function is connected to the angular clustering by

$$w(\theta) = \int dz N^2(z) \frac{dr}{dz} \int dx \xi \left( \sqrt{x^2 + r^2 \theta^2} \right), \quad (3)$$

where  $N(z)$  is the normalized redshift distribution of the galaxy sample,  $r$  is the comoving radial distance at redshift  $z$  and  $dr/dz = (c/H_0)/\sqrt{\Omega_m(1+z)^3 + \Omega_\Lambda}$ . The photometric redshift distribution is roughly a top-hat function for  $2.0 < z < 2.8$ . However, photometric redshift uncertainties are important in estimating the true underlying redshift distribution. Unless specified, we use the estimated true redshift distribution of the sample used by Q08 (kindly provided by R. Quadri). For this  $N(z)$ , the redshift distribution peaks at  $z = 2.3$  but contains significant wings out to  $z \sim 1.5$  and  $z \sim 3.3$  (see Figure 3 in Q08 for comparison). The amplitude of the  $w(\theta)$  is somewhat sensitive to the choice of  $N(z)$ ; for the same  $\xi(r)$ , using the photometric  $N(z)$  increases the amplitude of  $w(\theta)$  by  $\sim 20\%$ , independent of scale. Although the uncertainty in  $N(z)$  is a source of error in the theoretical calculations, we will show that it is subdominant to the sample variance of the observations themselves. In practice, we calculate  $\xi(r)$  at the peak of  $N(z)$ ,  $z = 2.3$ , and implement that function in equation (3). Q08 recalculate  $\xi(r)$  at each  $z$  using the redshift-dependent halo statistics with a fixed HOD. The assumption that the HOD is fixed in redshift is likely wrong to some degree but cannot be quantified, thus it is not necessarily more robust to recalculate  $\xi(r)$  as a function of redshift. In practice, we find that there are negligible differences between the two approaches.

Our motivation for using an analytic model to calculate galaxy clustering, rather than using one of the simulations, is two-fold. First, it frees us to use our desired cosmological model. Second, it ameliorates any numerical issues of spatial resolution; the Q08 clustering measurements extend down to  $\sim 0.02 h^{-1} \text{Mpc}$  (comoving at  $z = 2.3$ ), which is below the limit at which subhalos can be identified in the simulations. Figure 1b demonstrates the veracity of our analytic model. The points show the clustering of subhalos in the L120 box while the solid curve shows the clustering obtained from the analytic model using the HOD in Figure 1a (shifted to the proper mass scale, and using the cosmology of the L120 box). The good agreement with the simulation results demonstrate the robustness of our analytic model.

### 2.3. Breaking Galaxies into Red and Blue

DRGs do not comprise a luminosity-threshold sample of galaxies; the luminosity functions of Marchesini et al. (2007) demonstrate that even at the brightest end, DRGs only account for roughly half of all galaxies. Our model for the fraction of central galaxies that are DRGs has a mass-dependence of the form

$$f_{\text{Rcen}}(M) = f_{\text{Rmax}} \exp \left[ \frac{-\kappa M_{\text{min}}}{M - M_{\text{min}}} \right]. \quad (4)$$

Equation (4) implies that all galaxies at  $M = M_{\text{min}}$  are blue (non-DRGs), and that the fraction of DRGs smoothly increases to an asymptotic value of  $f_{\text{Rmax}}$  at high masses. If  $\kappa = 0$ , then  $f_{\text{Rcen}} = f_{\text{Rmax}}$  at all masses and central DRGs are a random subsample of all central galaxies. Formally, the parameter  $\kappa$  is the fractional increase in halo mass with respect to  $M_{\text{min}}$  for  $f_{\text{Rcen}}$  to reach  $1/e$  of the asymptotic value  $f_{\text{Rmax}}$ . In lieu of  $\kappa$ , we will refer to a physically more interesting quantity, the ratio between the mean halo mass for central DRGs and the mean halo mass for all central galaxies,

$$\mu_{\text{cen}} = \frac{\int_{M_{\text{min}}}^{\infty} dM (dn/dM) M f_{\text{Rcen}}(M)}{\int_{M_{\text{min}}}^{\infty} dM (dn/dM) M}, \quad (5)$$

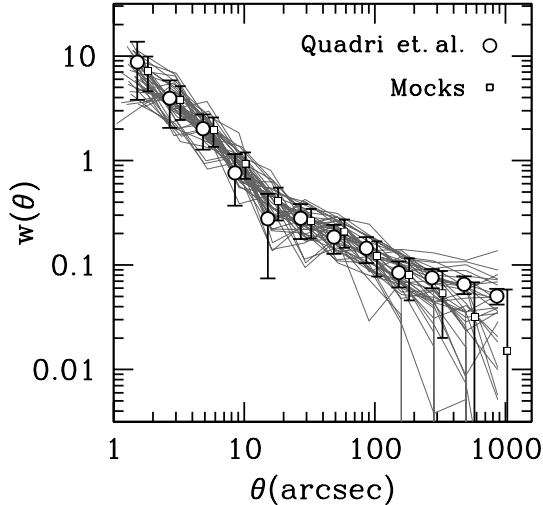


FIG. 2.— Dispersion of the clustering from the  $15^2$  mock catalogs. The thin gray curves show  $w(\theta)$  for a random 18% of the mocks. The open circles are the Q08 data and errors. The open squares represent the mean (corrected for the integral constraint) and dispersion among the mocks. The squares have been shifted slightly for clarity. For all calculations, the covariance of the mocks is used as the errors on the Q08 data.

where  $dn/dM$  is the halo mass function.

For satellite galaxies we stipulate that a constant fraction  $f_{R\text{sat}}$  of satellites are DRGs, independent of mass. A more physical model may have a mass-dependent satellite red fraction, but with the large errors on the given data, a three-parameter model is a reasonable first step.

An important uncertainty in modeling DRG clustering is the uncertainty in the number density of such objects. Our model for the DRG fraction has three free parameters ( $\kappa$ ,  $f_{R\text{max}}$ , and  $f_{R\text{sat}}$ ), but  $\bar{n}_{\text{DRG}}$  reduces the degrees of freedom by one. However, given the small sample size, the error in  $\bar{n}_{\text{DRG}}$  is non-negligible and must be taken into account when modeling the data. We will address this in the following section.

#### 2.4. Error Estimation

Q08 obtain error bars through bootstrap resampling of their data, where each bootstrap sample draws from the distribution of all galaxies. This method is good for estimating errors due to shot noise but not due to cosmic variance. The measurements of  $w(\theta)$  are taken out to  $\sim 1200$  arcsec (0.33 deg), close to half the width of the field (0.84 deg). Given the volume of the field, roughly  $2.2 \times 10^6 (h^{-1}\text{Mpc})^3$  (about the volume of a  $(130 h^{-1}\text{Mpc})^3$  cube), cosmic variance is important for modeling the data at large-scales.

To estimate the errors on the Q08 data, we construct mock catalogs by populating the halos in a large-volume simulation (L1000 listed in Table 1). The simulation itself does not resolve substructure, so we use the analytic  $\langle N \rangle_M$  from Figure 1 to populate the halos in the simulation. Central galaxies are placed at the center of mass of the halo and satellite galaxies are placed randomly, assuming a density profile that follows that of Navarro et al. (1996). Halos are identified in the simulation using the friends-of-friends technique (e.g., Davis et al. 1985). Due to the low mass resolution of the simulation, we use halos down to 10 particles. This is not ideal, but the large-scale bias of these halos matches theoretical expectations, thus the mock-to-mock variations of these halos is accu-

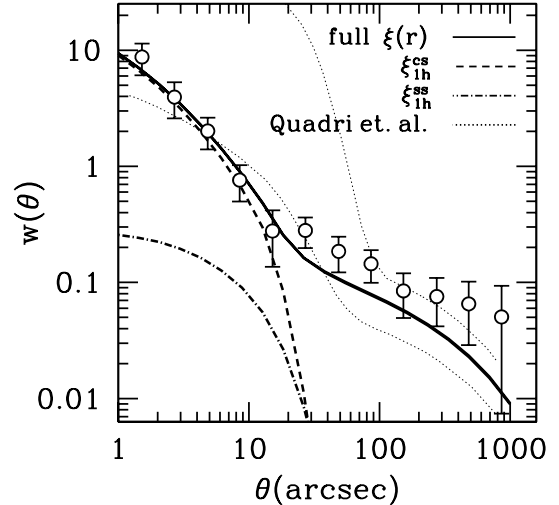


FIG. 3.— Comparison of models to  $w(\theta)$  measurements. The solid curve shows the best-fit HOD model that matches the  $w(\theta)$  and number density of DRGs. The dashed and dashed-dot curves show the breakdown of the one-halo term into central-satellite pairs ( $\xi_{1h}^{\text{cs}}$ ) and satellite-satellite pairs ( $\xi_{1h}^{\text{ss}}$ ). The thin dotted curves are the two fits presented in Q08.

rate (Hu & Kravtsov 2003). To determine the DRG fraction, we use a model with parameters  $\kappa = 0.65$  and  $f_{R\text{sat}} = 0.64$ , yielding a value of  $f_{R\text{max}} = 0.95$ . (This was the best-fit model from fitting the Q08 data using the Q08 error bars and a constant  $N(z)$  from  $2 < z < 2.8$ .)

We use the simulation output at  $z = 2.5$ .<sup>2</sup> The comoving distance from  $2 < z < 3$  is roughly 1 comoving  $h^{-1}$  Gpc, allowing us to fully incorporate the the redshift depth of the Q08 photometric sample. We use a redshift distribution that is constant from  $z = 2$  to  $z = 2.8$ , and zero at higher and lower redshift. At  $z = 2.8$ , 0.84 deg of arc is 64 comoving  $h^{-1}$  Mpc, thus we are able to create  $15^2 = 225$  mocks.

A random sample of 18% of the mocks are compared to the Q08 data in Figure 2. The data has been corrected for the integral constraint. We also perform the integral constraint correction for the correlation functions from the mocks by adding a constant. The constant is computed as the difference between the mean correlation function of all mocks and the correlation function measured from the entire box. The agreement between the mocks and the Q08 data at large scales is artificially enhanced due to a number of reasons.

The narrow  $N(z)$  function increases the amplitude of  $w(\theta)$ , and with the smaller error bars at large scales the best-fit model has a lower number density, yielding a higher bias. The FOF halos with low particle numbers exhibit somewhat stronger scale-dependence than that seen in Tinker et al. (2009), which helps the fit at  $\theta \sim 20''$ . However, for the purpose of estimating cosmic variance the most important criterion is producing mocks the reproduce the data on most scales. The large-scale clustering of the mock DRG samples is consistent with the data given the sample variance at less than  $1 - \sigma$ . At  $\theta \lesssim 50$  arcsec, the bootstrap errors of Q08

<sup>2</sup> Using a single redshift output rather than a full lightcone makes negligible difference in the clustering. As redshift decreases, the amplitude of dark matter clustering increases with the growth factor, but if the HOD is fixed (as assumed here and in all HOD fits to  $w(\theta)$  data) then the bias at the mean mass scale of the galaxies decreases in such a way as to nearly cancel the change in dark matter clustering.

are quite accurate in recovering the error, but the error bar on the  $\theta = 10^3$  arcsec datum is underestimated by a factor of 5. Henceforth, we use the dispersion among the mocks as the diagonal errors on the Q08 data. We note that we use the dispersion as an absolute error, not a fractional error. Because  $w(\theta)$  is a projected quantity, the data points are highly correlated. Our large number of mocks allows us to robustly calculate the covariance matrix for the Q08 sample. For all model fitting we use the covariance matrix. We also note that Q08 have an additional datum at  $\theta = 1400$  arcsec. Although the measured value of  $w(\theta)$  is significantly lower than the other data points, we do not use this point because sample variance renders it essentially useless.

Guo & White (2008) use the Millennium semi-analytic model to make similar mock samples to compare to the Q08 data (a simulation 1/8 the volume of our L1000 simulation). The dispersion of their 48 mocks is comparable to Figure 2, but their mean correlation function is significantly lower than the Q08 data, even at small scales. Even with this discrepancy, 6 of their 48 mocks match the large-scale data up to the data at  $\theta < 10^3$ , which is roughly a  $1-\sigma$  result and consistent with our conclusions.

The variance in the number density from the mocks is 11%, somewhat better than the 18% uncertainty on  $\bar{n}_{\text{DRG}}$  from Marchesini et al. 2007, owing to the larger sample size. We use this 11% uncertainty when modeling the clustering.

### 3. RESULTS

#### 3.1. Fitting the Quadri et al. data

We use a Monte Carlo Markov Chain (MCMC) analysis to determine the best-fit model parameters as well as their uncertainties. Using  $w(\theta)$  and  $\bar{n}_{\text{DRG}}$ , the model with the minimum  $\chi^2$  has parameters  $f_{\text{Rsat}} = 0.69$ ,  $f_{\text{Rmax}} = 0.99$ , and  $\kappa = 0.48$ , yielding a number density of  $6.4 \times 10^{-4}$  and  $\mu_{\text{cen}} = 1.46$ . The  $\chi^2$  for this model is 7.0 with 13–3 degrees of freedom. Figure 3 compares our best-fit model with the Q08 data. At most scales the model is within the  $1-\sigma$  errors. The highly correlated nature of the data in the two-halo regime reduces the significance of the offset between the model and the data. The thin dotted lines show the two models presented in Q08. The upper curve, which matches the data at large scales, diverges rapidly from the data at  $\theta < 100$  arcsec because nearly all galaxies in this model are satellites in high-mass halos. The lower curve matches the data adequately on small scales, but is significantly below the data in the two-halo term, even with our new errors estimates.

The differences between these two analyses are driven by the treatment of the second moment at small scales and the choice of halo bias models at large scales. The calculations of Q08 are based on the model of Hamana et al. (2004) (also used by Lee et al. 2006 to model the clustering of LBGs, and similar to the model of Bullock et al. 2002). In this formulation, the mean occupation function is a simple power law of the form

$$\langle N \rangle_M = \begin{cases} (M/M_1)^\beta & \text{if } M \geq M_{\text{min}} \\ 0 & \text{if } M < M_{\text{min}}. \end{cases} \quad (6)$$

Even though equation (6) has one fewer free parameter than our  $\langle N \rangle_M$  in §2.2, it has significantly less freedom because it does not parameterize centrals and satellites separately. It is well known that assuming entirely Poisson fluctuations around  $\langle N \rangle_M$  produces clustering results that cannot match observations; the second moment is too high at low  $\langle N \rangle_M$

(see, e.g., Benson et al. 2000; Seljak 2000; Scoccimarro et al. 2001; Berlind & Weinberg 2002). In the HOD model of §2, the sub-Poisson scatter is a natural consequence of parameterizing the centrals and satellites separately; the second moment of the satellites is always Poisson, but when  $\langle N_{\text{sat}} \rangle_M$  falls below unity the total distribution of pairs becomes sub-Poisson because there is no scatter (or only a nearest-integer distribution) of central galaxies (see Kravtsov et al. 2004; Zheng et al. 2005). In addition, the separation distribution of central-satellite pairs is different than satellite-satellite pairs. In the former, the pair distribution follows the halo density profile. In the latter, the pair distribution is represented by the density profile convolved with itself. In galaxy distributions with high satellite fractions (say,  $\sim 30\%$  for  $L < L_*$  galaxies), the overall shape of the one-halo term will differ from samples with a low fraction of satellites (such as LRGs, DRGs, or any other commensurately bright sample that populates the high-mass end of the halo mass function; see the discussion in the Appendix A of Zheng et al. 2008).

In equation (6) there is no explicit separation of central and satellite galaxies. Thus, sub-Poisson fluctuations are specified in the model *ad-hoc* when  $\langle N \rangle_M < 1$ . More importantly, the model specifies a binary switch between radial pair distributions; at  $\langle N \rangle_M \geq 1$ , the entire one-halo term is calculated assuming a satellite-satellite profile even though, at that mass scale, almost *all* pairs are still central-satellite. In Figure 3, the relative contribution of central-satellite pairs,  $\xi_{\text{1h}}^{\text{cs}}(r)$ , and satellite-satellite pairs,  $\xi_{\text{1h}}^{\text{ss}}(r)$ , to the one-halo term is shown with the dashed and dot-dashed curves, respectively. At all scales  $\xi_{\text{1h}}^{\text{cs}}(r)$  dominates because the overall satellite fraction of this sample is low (16%); although satellites dominate the pair counts at  $M \gtrsim 2M_1$ , the number of halos at that mass is nearly negligible because  $M_1$  is on the exponentially-falling tail of the mass function for this sample. One can see that the shape of the one-halo term from the Hamana et al. (2004) model is the same as  $\xi_{\text{1h}}^{\text{ss}}(r)$ . This gives the one halo term a higher amplitude and larger radial extent than a model in which the two one-halo terms are properly weighted. Thus, to match at small scales, the best-fit model forces the large-scale clustering lower than it otherwise would be.

The differences between Q08 and this work at small scales do not entirely account for the differences at large scales. Half the difference can be accounted for by the choice of large-scale bias. Q08 use the bias model of Sheth et al. (2001) (hereafter SMT), which was calibrated on small-volume simulations. There is debate in the literature over the accuracy of the SMT bias function at high masses (relative to the non-linear mass scale  $M_*$ ) compared to the spherical collapse model (e.g., Cole & Kaiser 1989; Mo & White 1996), which predicts stronger bias at these mass scales (see Cohn & White 2008; Reed et al. 2008). Our model is intermediate between these two models and agrees perfectly with the bias of the Millennium simulation shown in Gao et al. (2005). Our new bias prescription increases the large-scale bias of the galaxy sample by 10% relative to SMT, increasing the large-scale amplitude of  $\xi(r)$  by 20%. The results of Figure 1b also show that our bias prescription is adequately describing the clustering of halos in the L120 simulation. Using the SMT bias function, our best-fit model has a  $\chi^2 = 10.0$ , while the Q08 model yields  $\chi^2 = 26.4$ . Using the SMT bias function has no effect on the parameter constraints in §3.3. For comparison, using diagonal errors only results in  $\chi^2$  values of 10.9 for the best-fit model, 19.5 when using SMT bias, and 32.0 for the Q08 model.

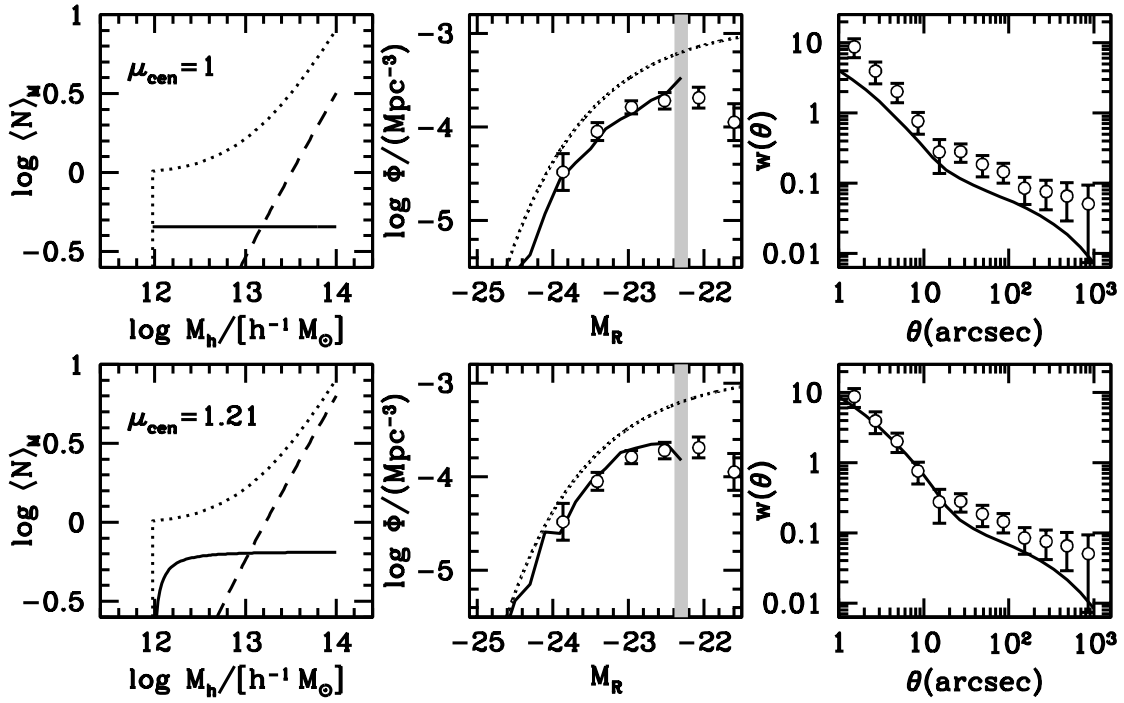


FIG. 4.— Two examples of the combined constraints of  $w(\theta)$  and  $\Phi_{\text{DRG}}$ . The top row shows results from assuming that DRGs are a random sample of all galaxies. The top left panel shows the HOD; the solid curve shows  $\langle N_{\text{cen}} \rangle_M$  for DRGs, and the dashed line shows  $\langle N_{\text{sat}} \rangle_M$  for DRGs. The dotted curve shows  $\langle N \rangle_M$  for all galaxies for comparison. The middle panel shows the luminosity function of Marchesini et al. (2007) (points with errors). The solid line is the model luminosity function. The dotted line is the luminosity function for all galaxies. The thick solid line is the completeness limit of the Q08 data. The right panel is the clustering of DRGs. The points represent the Q08 data, while the curve is the model prediction from the HOD in the far left panel. *Bottom row:* The best-fit model from the combined constraints of  $w(\theta)$  and  $\Phi_{\text{DRG}}$ . The mean mass of central DRGs is 21% higher than the overall sample of central galaxies ( $\sim 40\%$  higher than non-DRG central galaxies). This model produces a better fit to both the luminosity function and  $w(\theta)$ .

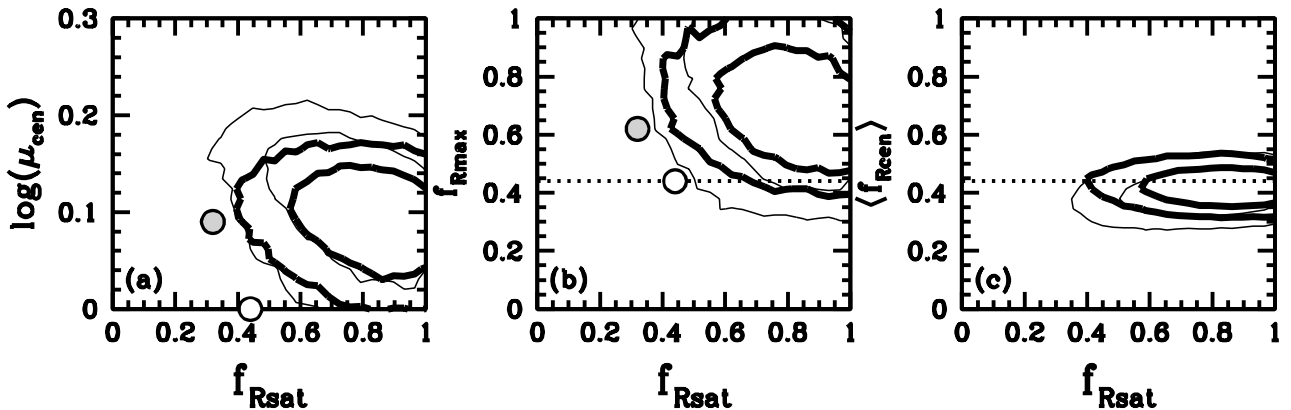


FIG. 5.— Panel (a): Constraints on  $f_{\text{Rsat}}$  and  $\mu_{\text{cen}}$  from the MCMC chains. Thick contours represent the 1- $\sigma$  and 2- $\sigma$  constraints using both  $w(\theta)$  and  $\Phi_{\text{DRG}}$ . Thin contours correspond to using  $w(\theta)$  alone. The gray dot represents the value  $f_{\text{Rsat}}$  obtained if equation (4) were applied to the subhalos. The white dot represents a model in which DRGs are a random sample of all galaxies. Panel (b): Constraints on  $f_{\text{Rsat}}$  and  $f_{\text{Rmax}}$ . Contours are as in panel (a). The dotted line indicates the overall fraction of DRGs, 44%. Panel (c) shows the constraints on  $f_{\text{Rsat}}$  and  $\langle f_{\text{cen}} \rangle$ , the mean central DRG fraction integrating over all halos.

### 3.2. Including the Luminosity Function

To a first approximation, rest-frame  $R$ -band absolute magnitude should be monotonically correlated with dark matter halo and subhalo mass. This is borne out by the SHAM results of Conroy et al. (2006), and it is further supported by the comparison between SHAM and the clustering of  $z \sim 2$  star-forming galaxies (Conroy et al. 2008). By construction, the luminosity function of the galaxies in our model exactly follow that measured by Marchesini et al. (2007) for all galaxies (DRG and non-DRG). For each galactic halo, the luminosity of the galaxy within it is set by matching the cumulative halo abundance to the cumulative luminosity function. We can combine the luminosity set in this way with the mass-dependent DRG occupation function described in §2.2 to create a DRG luminosity function, which has also been measured by Marchesini et al. (2007). To do this, we use the halos and subhalos identified in the L160 simulation. Each halo has a luminosity obtained through the abundance-matching method. Whether or not the galaxy is a DRG is decided by Monte Carlo based on  $f_{R\text{cen}}(M)$  and  $f_{R\text{sat}}$ .

Figure 4 shows two examples of the combined constraints of  $w(\theta)$ ,  $\bar{n}_{\text{DRG}}$  and  $\Phi_{\text{DRG}}$ <sup>3</sup>. In the top row, we show a model in which DRGs are simply a random sample of all galaxies. Thus  $\mu_{\text{cen}} = 1$  ( $\kappa = 0$ ) and  $f_{R\text{max}} = f_{R\text{sat}} = 0.44$ . The occupation function for DRGs is the same as  $\langle N \rangle_M$  for all galaxies but shifted down by 0.44. The luminosity function produced by this model is in good agreement with the observations, but the clustering is clearly inconsistent with the measurements, both at large and small scales. The bottom row presents the results from our best-fit model from this combined approach. In this model,  $\kappa = 0.18$ ,  $f_{R\text{sat}} = 0.91$  and  $f_{R\text{max}} = 0.66$ , yielding  $\mu_{\text{cen}} = 1.21$ . This shift of the mass scale of central DRGs produces a noticeable increase in the large-scale bias of  $w(\theta)$ . The increased fraction of red satellites increases the amplitude of one-halo term to agree well with the data. The luminosity function of this model agrees essentially perfectly with observations, producing the right number of high-luminosity objects while still matching the faint end down to the completeness limit of the Q08 sample. With 17-3 degrees of freedom, this model yields  $\chi^2/\nu = 7.7/14$ .

### 3.3. Parameter Constraints

We can use the observational data to place constraints on  $\kappa$ ,  $f_{R\text{sat}}$ , and  $f_{R\text{max}}$ . Figure 5 shows the results from the MCMC chains. The thick contours are the 1- and 2- $\sigma$  constraints using  $w(\theta)$ ,  $\bar{n}_{\text{DRG}}$ , and  $\Phi_{\text{DRG}}$ , while the thin contours represent results using only  $w(\theta)$  and  $\bar{n}_{\text{DRG}}$ . Figure 5a plots the constraints on the  $f_{R\text{sat}}-\mu_{\text{cen}}$  plane. It is clear from Figure 4 that a large fraction of satellites must be red in order to match the clustering; the best-fit value of  $f_{R\text{sat}} = 0.9$  and the 2- $\sigma$  lower limit is  $\sim 50\%$  when marginalizing over other parameters. Ratios of the halo mass scale between central DRGs and all central galaxies above  $\mu_{\text{cen}} \approx 1.5$  are excluded at  $> 2-\sigma$ , but a model in which  $\mu_{\text{cen}} = 1$  (i.e., central DRGs are a random subsample of all central galaxies) is also excluded at roughly 2- $\sigma$ .

Figure 5b shows the parameter constraints in the  $f_{R\text{sat}}-f_{R\text{max}}$  plane. The dotted line indicates the mean DRG fraction. This figure highlights the benefit of using the luminosity function as an additional constraint on the models. When considering

<sup>3</sup> We include both  $\bar{n}_{\text{DRG}}$  and  $\Phi_{\text{DRG}}$  as independent data because  $\Phi_{\text{DRG}}$  does not necessarily include  $\bar{n}_{\text{DRG}}$ . We find little difference in parameter constraints when excluding  $\bar{n}_{\text{DRG}}$ .

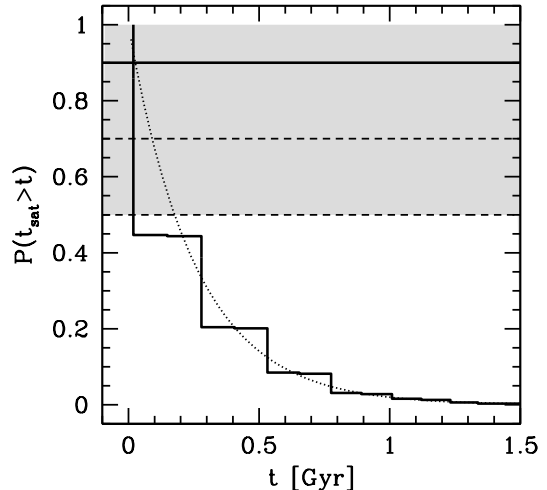


FIG. 6.— Cumulative distribution of subhalos with accretion times (time since accretion) longer than  $t$ . Histogram shows the numerical data. The dotted line is a fitting function of the form  $\exp(-3.9t)$ . The shaded region shows the 2- $\sigma$  constraints on the fraction of satellites that are required to be DRGs to match the data. The thick solid line is the best-fit value; dashed lines represent the 1- and 2- $\sigma$  confidence levels after marginalized over other parameters.

$w(\theta)$  and  $\bar{n}_{\text{DRG}}$  only, the model strives to push the large-scale bias as high as possible. This results in a best-fit  $f_{R\text{max}}$  of unity, implying all halos above  $M \sim 10^{12.5} h^{-1} M_{\odot}$  contain a DRG at their center. However, this overproduces the number of bright DRGs at the expense of the low-luminosity end. Using  $w(\theta)$  and  $\Phi_{\text{DRG}}$ , the best-fit value of  $f_{R\text{max}}$  is 0.66.

Figure 5c shows the constraints on red satellite fraction and the mean red central fraction averaged over all halos. The constraints in all three panels imply that a higher fraction of satellites than centrals must be red in order to match the data. (We remind the reader that  $f_{R\text{max}}$  is the asymptotic value of  $f_{R\text{cen}}(M)$ ; at fixed  $f_{R\text{sat}}$ , the higher the value of  $f_{R\text{max}}$ , the lower the red fraction at lower halo masses in order to keep the number of central DRGs constant. The overall red central fraction will usually be near 44% because the contribution of satellites is small.) The gray circle in Figures 5a and 5b shows the  $f_{R\text{sat}}$  that results if we apply the mass-dependent  $f_{R\text{cen}}(M)$  to the subhalos themselves for the best-fit value of  $\kappa$ . Because subhalos have a lower mean mass than parent halos, in this case the fraction of red satellites is less than the fraction of red centrals if they have the same duty cycle. Thus, using this model, the fraction of red satellites is 32%, a value that is clearly outside the 2- $\sigma$  contour.

## 4. DISCUSSION

### 4.1. Satellite DRGs

The results from Figure 5 imply that the physical processes that turn a galaxy red, either by creation of dust or through star formation history, are different for centrals and satellites at  $z > 2$ . At low redshift such a scenario is expected; after accretion, gas is ram-pressure stripped and star formation in satellites is “quenched”. However, the situation at high redshift is quite different; the universe at  $z = 2.3$  is only  $\sim 2.9$  Gyr old in our cosmology, and most mergers of small halos onto bigger ones have occurred quite recently. Thus, one would naively expect that red satellites were red before they were accreted

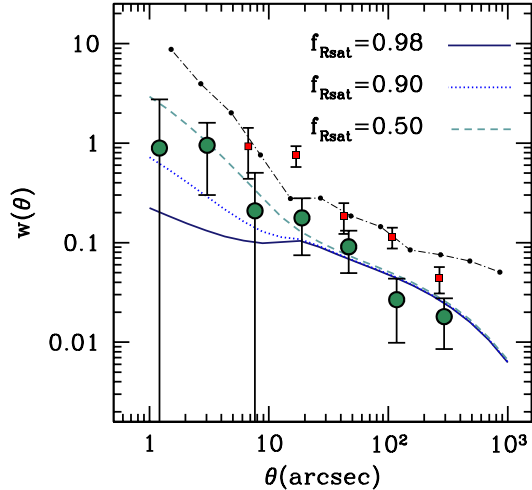


FIG. 7.— Clustering of blue galaxies (non-DRGs) at the same redshift as the Q08 sample. Large circles and their errors are taken from Quadri et al. (2007), which show the clustering of  $J-K < 2.3$  galaxies from a smaller sample. The lines are HOD predictions for the clustering of non-DRGs from the best-fit value of  $\mu_{\text{cen}}$  but with varying red satellite fractions. The dotted line is the prediction of the overall best-fit model (bottom row of Figure 4.) The small squares are the measurement from Quadri et al. (2007) for DRGs, which are consistent with the Q08 data (black circles connected by the dash-dot curve).

(or would have become red regardless of accretion); i.e., that the processes that make a galaxy red are driven primarily by the mass of its galactic halo rather than their position as an accreted object. Such a scenario is difficult to reconcile with the Q08 data.

Figure 6 shows the cumulative distribution of satellite ages (i.e., time since they were accreted) for subhalos above the minimum mass threshold of  $\langle N \rangle_M$  in the simulations. Because the accretion times are discretized, the dotted line is a fitting function of the form  $\exp(-3.9t)$  that allows for quick interpolation between the points. Naively we may infer a quenching time scale based on the fraction of satellites being DRGs (e.g., 200 Myr from the  $2\text{-}\sigma$  line in Fig. 6), but this makes the strong assumption that all satellite DRGs have little to no star formation. Let us assume that 30% of DRGs have significantly attenuated star formation (Labbé et al. 2005), and 32% of DRG satellites were classifiably DRGs before accretion (from the gray dot in Figure 5). Using the best-fit value of  $f_{\text{Rsat}} = 0.9$ ,  $0.9 \times (1 - 0.32) \times 0.3 = 0.18$  is the fraction of all galaxies that have their star formation attenuated through satellite accretion. From Figure 6, a star formation quenching timescales of 450 Myr is obtained. This is in clear contrast with results from low redshift, where the exponential timescale for the reduction of star formation in satellites is closer to 2-2.5 Gyr (Wang et al. 2006; Kimm et al. 2008). These results can be brought into better agreement if the exponential timescale scales with the dynamical time of the galactic halo, reducing the  $e$ -folding time by  $(1+z)^{1.5} = 6$ , depending on the number of  $e$ -folds required to be considered “red and dead”. Robust conclusions are difficult to establish given the uncertainty in the fraction of DRGs with no star formation, uncertainty in how that fraction is distributed between centrals and satellites, and the uncertainty in  $f_{\text{Rsat}}$ .

Regardless of current star formation rates, it is also difficult

to reconcile the high overall fraction of satellite DRGs with satellite accretion timescales. While there is a physical mechanism that halts star formation for satellite galaxies, accretion onto a larger halo cannot account for excess  $K$ -band emission from an advanced (multi-Gyr) stellar population that is part of the definition of a DRG. Irrespective of accretion time, the old stars were formed before the galaxy became a satellite galaxy. Thus the satellite had to know it would be accreted well beforehand. For  $z = 2.3$   $10^{13} h^{-1} M_{\odot}$  halos, their average mass was  $\sim 1/10$  at  $z \sim 5$  (Wechsler et al. 2002), but their rapid growth and high relative mass can influence their larger environment and the smaller halos that will eventually be accreted at later times (Wang et al. 2007; Hahn et al. 2008; Dalal et al. 2008). These lower-mass halos within the lagrangian radius of the large halo will have formed earlier and possibly have older stellar populations than a halo of the same mass which formed outside the lagrangian radius of a large halo. By  $z \approx 2.3$ , these early-forming halos have become satellites in the nearby high-mass halos.

It would be perhaps too coincidental that this effect would *only* alter the formation of halos that would become subhalos at the epoch of the Q08 sample, especially given that most accretion events are very recent. High mass halos at  $z = 2.3$  will continue to rapidly grow and alter the formation trajectories of smaller halos around them, inducing assembly bias—the correlation between halo occupation and large-scale environment at fixed halo mass—cited by Q08 to explain the high clustering amplitude of DRGs. If this assembly bias extends to halos outside the virial radii of  $M \gtrsim 10^{13} h^{-1} M_{\odot}$  halos (but within their vicinity), the large-scale clustering of DRGs would be enhanced, supporting the conclusions of Q08. The data do not require any assembly bias to fit the large scale  $w(\theta)$ , but it is implied by the high fraction of satellite galaxies being of DRGs.

Recent developments in stellar population synthesis, specifically the inclusion of thermally-pulsating AGB stars, may alleviate some of the tension between the age of the universe at  $z = 2.3$  and the stellar population ages required to reproduce the observed colors of DRGs (Tonini et al. 2008), although this mechanism is not related to the high fraction of satellites being DRGs or the fraction of DRGs without star formation.

#### 4.2. Central Galaxies

For central galaxies, the luminosity function alone supports a model in which DRGs are a random subsample of the halos occupied by bright galaxies. In contrast, the clustering of DRGs supports a model in which massive halos ( $M \gtrsim 10^{12.5}$ ) *only* house DRGs at their centers. Considered together, a more intermediate picture becomes clear in which massive halos host DRGs  $\sim 2/3$  of the time, in good agreement with the mass-selected sample of van Dokkum et al. (2006). We have made two strong assumptions when predicting  $\Phi_{\text{DRG}}$  from our models: 1) that there is no scatter in the relation between halo mass and luminosity, and 2) that mass and  $R$ -band magnitude are monotonically correlated regardless of galaxy color. For 1), we note that scatter does not change the predicted  $\Phi_{\text{DRG}}$  when  $\mu_{\text{cen}}$  and  $f_{\text{Rmax}}$  are high; these models are excluded when using  $\Phi_{\text{DRG}}$  (cf, Figure 5b). In such models *all* high-mass halos contain DRGs at their centers, thus scatter only changes what halo each DRG lives in and not the distribution of DRG luminosities on the bright end. Significant scatter between halo mass and luminosity at low luminosities would decrease the observed amplitude of the correlation function, contrary to the observations (unless assembly bias is canceling out this ef-



fect). For 2), with the given data we cannot rule out a model in which red galaxies and blue galaxies of the same  $R$  magnitude occupy halos with substantially different masses. Our model makes a clear prediction for the clustering of blue galaxies that is sensitive to this assumption. For a complete model, the clustering of blue and red galaxies should be modeled simultaneously.

Figure 7 shows the clustering of non-DRGs ( $J-K < 2.3$ ) from Quadri et al. (2007), a distinct and much smaller sample of galaxies than Q08. The three lines are predictions from our best-fit value of  $\kappa = 0.18$  for different values of  $f_{R\text{sat}}$ . At large scales, the measured amplitude of  $w(\theta)$  is consistent with our model predictions. This agreement supports the second assumption above and argues against significant assembly bias in the DRG population; if the clustering of DRGs is enhanced by assembly bias then the clustering on non-DRGs must be suppressed by the same effect. At small scales, there is a signature of one-halo clustering in the blue galaxies. A model with nearly no blue satellites appears to be difficult to reconcile with the observations, but these data cannot distinguish between models in which 90% and 50% of the satellites are red. Because this is a different galaxy sample from Q08 with a different redshift distribution, the comparison in Figure 7 is meant to be qualitative only. We note, however, that the DRG clustering from Quadri et al. (2007) is consistent with that measured in Q08 (dash-dot curve and squares in Figure 7). Measurements of the clustering of blue galaxies within the Q08 sample will enhance our constraints both for halo occupation and for assembly bias. The relative bias between red and blue galaxies within the same field can also shed light on the issue of assembly bias. Because they would be measured from the same volume, large-scale modes would affect the clustering of both red and blue galaxies in the same way and the relative bias is therefore independent of cosmic variance (Seljak 2008; McDonald & Seljak 2008). Assembly bias, on the other hand, would increase the clustering difference between red and blue subsamples.

## 5. CONCLUSIONS

The clustering of DRGs measured by Q08 can be adequately fit by standard halo occupation models. With proper estimates of the cosmic variance at large scales and a more robust implementation of the HOD, our best-fitting model has  $\chi^2/\nu < 1$ . Thus, from the large-scale clustering alone there is no compelling evidence for assembly bias in the halo occupation of DRGs. The high clustering amplitude of DRGs has been measured by other authors (Daddi et al. 2003; Grazian et al. 2006), but the Daddi et al. (2003) data is fully described by HOD modeling as well (Zheng 2004). Given that the Q08 sample is by far the largest at present, the inclusion of other currently available data sets is not likely to change our conclusions, though cosmic variance is still an important systematic on large scales.

## APPENDIX

### A. HALO BIAS

The large-scale bias of halos used in this paper is based on the spherical overdensity halo catalogs of Tinker et al. (2008a). The full results for both large-scale bias and scale-dependent bias as a function of halo overdensity will be given elsewhere (Tinker et al. 2009). In the Tinker et. al. results, the fitting function for large-scale bias is

$$b(\nu) = 1 - A \frac{\nu^a}{\nu^a + \delta_c^a} + B\nu^b + C\nu^c. \quad (\text{A1})$$

where  $\nu = \delta_c/\sigma(M)$ ,  $\delta_c = 1.686$  and  $\sigma$  is the linear matter fluctuations within the lagrangian radius of a halo of mass  $M$ . For

To fit the prominent break in the  $w(\theta)$  between the two-halo and one-halo terms, a large fraction of satellite galaxies above the relevant luminosity threshold are required to be DRGs. The best-fit model has a red satellite fraction,  $f_{R\text{sat}}$ , of nearly unity, with a  $2-\sigma$  lower limit of 50%. This implies that the mechanisms through which DRGs form are more efficient (or more frequent) for satellite DRGs than for centrals, even though the accretion times of most subhalos are very recent at these epochs. At the best-fit value of  $f_{R\text{sat}} = 0.9$ , the timescale for star-formation quenching is roughly 450 Myr if quenching begins at the accretion time. Regardless of the star formation rates at  $z = 2.3$ , to produce the evolved stellar populations in satellite DRGs, subhalos are required to know that they will become subhalos well before they are accreted. This implies these object have some knowledge of the large-scale environment beyond that of their host halo mass (i.e. assembly bias), but further data is required to quantify the effect.

Down to the completeness limit of the Q08 data, central DRGs have an average halo mass that is 25% higher than the overall sample of galaxies (thus 50% higher than non-DRGs), but at the highest halo masses DRGs do not occupy all halos;  $\sim 1/3$  of the most massive halos at  $z = 2.3$  still contain blue galaxies at their centers.

Clustering data for high-redshift galaxies are becoming precise enough that realistic models for the occupation of galaxies within halos are important for robust interpretation. The approach taken in this work for modeling halo occupation is more realistic than earlier models that were developed to modeling high-redshift data (e.g. Bullock et al. 2002; Hamana et al. 2004). Explicit treatment of central and satellite galaxies is essential in modeling the transition regime between one and two halo pairs, which is particularly important as a constraining feature now that it is well measured in the data. The approach taken here, which combines information from simulations which resolve substructure to constrain the global sample with a flexible approach for modeling color dependence, is particularly powerful, and can also be applied to other color-selected galaxy samples.

We thank Ryan Quadri, Kyoung-Soo Lee, and Rik Williams for many helpful discussions. We also thank Martin White for comments on an earlier version of this draft. Much of the analysis was performed on the computing facilities at the Kavli Insitute for Cosmological Physics and the University of Chicago. The N-body simulations used here were run on the Columbia machine at NASA Ames. We are grateful to Anatoly Klypin for running these simulations and making them available to us. RHW was supported in part by the U.S. Department of Energy under contract number DE-AC02-76SF00515 and by a Terman Fellowship at Stanford University. ZZ gratefully acknowledges support from the Institute for Advanced Study through a John Bahcall Fellowship.

$\Delta = 200$  halos,  $A = 1.04$ ,  $a = 0.132$ ,  $B = 0.183$ ,  $b = 1.5$ ,  $C = 0.262$ , and  $c = 2.4$ .

## REFERENCES

- Benson, A. J., Cole, S., Frenk, C. S., Baugh, C. M., & Lacey, C. G. 2000, *MNRAS*, 311, 793
- Berlind, A. A. & Weinberg, D. H. 2002, *ApJ*, 575, 587
- Bullock, J. S., Wechsler, R. H., & Somerville, R. S. 2002, *MNRAS*, 329, 246
- Chen, J. 2007, *A&A*, in press, arXiv:0712.0003
- Cohn, J. D. & White, M. 2008, *MNRAS*, 385, 2025
- Cole, S. & Kaiser, N. 1989, *MNRAS*, 237, 1127
- Conroy, C., Shapley, A. E., Tinker, J. L., Santos, M. R., & Lemson, G. 2008, *ApJ*, 679, 1192
- Conroy, C., Wechsler, R. H., & Kravtsov, A. V. 2006, *ApJ*, 647, 201
- Cooray, A. & Sheth, R. 2002, *Phys. Rep.*, 372, 1
- Croton, D. J., Gao, L., & White, S. D. M. 2007, *MNRAS*, 374, 1303
- Daddi, E., Röttgering, H. J. A., Labbé, I., Rudnick, G., Franx, M., Moorwood, A. F. M., Rix, H. W., van der Werf, P. P., & van Dokkum, P. G. 2003, *ApJ*, 588, 50
- Dalal, N., White, M., Bond, J. R., & Shirokov, A. 2008, *ApJ*, 687, 12
- Davis, M., Efstathiou, G., Frenk, C. S., & White, S. D. M. 1985, *ApJ*, 292, 371
- Dunkley, J., Komatsu, E., Nolta, M. R., Spergel, D. N., Larson, D., Hinshaw, G., Page, L., Bennett, C. L., Gold, B., Jarosik, N., Weiland, J. L., Halpern, M., Hill, R. S., Kogut, A., Limon, M., Meyer, S. S., Tucker, G. S., Wollack, E., & Wright, E. L. 2008, *ApJS*, in press
- Förster Schreiber, N. M., van Dokkum, P. G., Franx, M., Labbé, I., Rudnick, G., Daddi, E., Illingworth, G. D., Kriek, M., Moorwood, A. F. M., Rix, H.-W., Röttgering, H., Trujillo, I., van der Werf, P., van Starkenburg, L., & Wuyts, S. 2004, *ApJ*, 616, 40
- Franx, M., Labbé, I., Rudnick, G., van Dokkum, P. G., Daddi, E., Förster Schreiber, N. M., Moorwood, A., Rix, H.-W., Röttgering, H., van de Wel, A., van der Werf, P., & van Starkenburg, L. 2003, *ApJ*, 587, L79
- Gao, L., Springel, V., & White, S. D. M. 2005, *MNRAS*, 363, L66
- Gao, L. & White, S. D. M. 2007, *MNRAS*, 377, L5
- Grazian, A., Fontana, A., Moscardini, L., Salimbeni, S., Menci, N., Giallongo, E., de Santis, C., Galozzi, S., Nonino, M., Cristiani, S., & Vanzella, E. 2006, *A&A*, 453, 507
- Guo, Q. & White, S. D. M. 2008, *ArXiv e-prints*, arXiv:0809.4259 [astro-ph]
- Hahn, O., Porciani, C., Dekel, A., & Carollo, C. M. 2008, *MNRAS*, submitted, arXiv:0803.4211 [astro-ph]
- Hamana, T., Ouchi, M., Shimasaku, K., Kayo, I., & Suto, Y. 2004, *MNRAS*, 347, 813
- Hu, W. & Kravtsov, A. V. 2003, *ApJ*, 584, 702
- Ichikawa, T., Suzuki, R., Tokoku, C., Uchimoto, Y. K., Konishi, M., Yoshikawa, T., Kajisawa, M., Ouchi, M., Hamana, T., Akiyama, M., Nishimura, T., Omata, K., Tanaka, I., & Yamada, T. 2007, *PASJ*, 59, 1081
- Kimm, T., Somerville, R. S., Yi, S. K., van den Bosch, F. C., Salim, S., Fontanot, F., Monaco, P., Mo, H., Pasquali, A., Rich, R. M., & Yang, X. 2008, *ArXiv e-prints*, arXiv:0810.2794 [astro-ph]
- Kochanek, C. S., White, M., Huchra, J., Macri, L., Jarrett, T. H., Schneider, S. E., & Mader, J. 2003, *ApJ*, 585, 161
- Kravtsov, A. V., Berlind, A. A., Wechsler, R. H., Klypin, A. A., Gottlöber, S., Allgood, B., & Primack, J. R. 2004, *ApJ*, 609, 35
- Kravtsov, A. V., Klypin, A. A., & Khokhlov, A. M. 1997, *ApJS*, 111, 73
- Kriek, M., van Dokkum, P. G., Franx, M., Quadri, R., Gawiser, E., Herrera, D., Illingworth, G. D., Labbé, I., Lira, P., Marchesini, D., Rix, H.-W., Rudnick, G., Taylor, E. N., Toft, S., Urry, C. M., & Wuyts, S. 2006, *ApJ*, 649, L71
- Labbé, I., Huang, J., Franx, M., Rudnick, G., Barmby, P., Daddi, E., van Dokkum, P. G., Fazio, G. G., Schreiber, N. M. F., Moorwood, A. F. M., Rix, H.-W., Röttgering, H., Trujillo, I., & van der Werf, P. 2005, *ApJ*, 624, L81
- Lee, K.-S., Giavalisco, M., Gnedin, O. Y., Somerville, R. S., Ferguson, H. C., Dickinson, M., & Ouchi, M. 2006, *ApJ*, 642, 63
- Lin, Y.-T., Mohr, J. J., & Stanford, S. A. 2004, *ApJ*, 610, 745
- Marchesini, D., van Dokkum, P., Quadri, R., Rudnick, G., Franx, M., Lira, P., Wuyts, S., Gawiser, E., Christlein, D., & Toft, S. 2007, *ApJ*, 656, 42
- Marín, F. A., Wechsler, R. H., Frieman, J. A., & Nichol, R. C. 2008, *ApJ*, 672, 849
- McDonald, P. & Seljak, U. 2008, *ArXiv e-prints*, arXiv:0810.0323 [astro-ph]
- Mo, H. J. & White, S. D. M. 1996, *MNRAS*, 282, 347
- Navarro, J. F., Frenk, C. S., & White, S. D. M. 1996, *ApJ*, 462, 563
- Quadri, R., van Dokkum, P., Gawiser, E., Franx, M., Marchesini, D., Lira, P., Rudnick, G., Herrera, D., Maza, J., Kriek, M., Labbé, I., & Francke, H. 2007, *ApJ*, 654, 138
- Quadri, R. F., Williams, R. J., Lee, K.-S., Franx, M., van Dokkum, P., & Brammer, G. B. 2008, *ApJ*, 685, L1
- Reed, D. S., Bower, R., Frenk, C. S., Jenkins, A., & Theuns, T. 2008, *ArXiv e-prints*, arXiv:0804.0004 [astro-ph]
- Scoccimarro, R., Sheth, R. K., Hui, L., & Jain, B. 2001, *ApJ*, 546, 20
- Seljak, U. 2000, *MNRAS*, 318, 203
- . 2008, *ArXiv e-prints*, arXiv:0807.1770 [astro-ph]
- Sheth, R. K., Mo, H. J., & Tormen, G. 2001, *MNRAS*, 323, 1
- Spergel, D. N., Bean, R., Doré, O., Nolta, M. R., Bennett, C. L., Dunkley, J., Hinshaw, G., Jarosik, N., Komatsu, E., Page, L., Peiris, H. V., Verde, L., Halpern, M., Hill, R. S., Kogut, A., Limon, M., Meyer, S. S., Odegard, N., Tucker, G. S., Weiland, J. L., Wollack, E., & Wright, E. L. 2007, *ApJS*, 170, 377
- Spergel, D. N., Verde, L., Peiris, H. V., Komatsu, E., Nolta, M. R., Bennett, C. L., Halpern, M., Hinshaw, G., Jarosik, N., Kogut, A., Limon, M., Meyer, S. S., Page, L., Tucker, G. S., Weiland, J. L., Wollack, E., & Wright, E. L. 2003, *ApJS*, 148, 175
- Tinker, J., Kravtsov, A. V., Klypin, A., Abazajian, K., Warren, M., Yepes, G., Gottlöber, S., & Holz, D. E. 2008a, *ApJ*, 688, 709
- Tinker, J. L., Conroy, C., Norberg, P., Patiri, S. G., Weinberg, D. H., & Warren, M. S. 2008b, *ApJ*, 686, 53
- Tinker, J. L., Weinberg, D. H., Zheng, Z., & Zehavi, I. 2005, *ApJ*, 631, 41
- Tinker, J. T. et al. 2009, in preparation
- Tonini, C., Maraston, C., Devriendt, J., Thomas, D., & Silk, J. 2008, *MNRAS*, submitted, arXiv:0812.1225 [astro-ph]
- van Dokkum, P. G., Förster Schreiber, N. M., Franx, M., Daddi, E., Illingworth, G. D., Labbé, I., Moorwood, A., Rix, H.-W., Röttgering, H., Rudnick, G., van der Wel, A., van der Werf, P., & van Starkenburg, L. 2003, *ApJ*, 587, L83
- van Dokkum, P. G., Quadri, R., Marchesini, D., Rudnick, G., Franx, M., Gawiser, E., Herrera, D., Wuyts, S., Lira, P., Labbé, I., Maza, J., Illingworth, G. D., Förster Schreiber, N. M., Kriek, M., Rix, H.-W., Taylor, E. N., Toft, S., Webb, T., & Yi, S. K. 2006, *ApJ*, 638, L59
- Wang, H. Y., Mo, H. J., & Jing, Y. P. 2007, *MNRAS*, 375, 633
- Wang, L., Li, C., Kauffmann, G., & De Lucia, G. 2006, *MNRAS*, 371, 537
- Wechsler, R. H., Bullock, J. S., Primack, J. R., Kravtsov, A. V., & Dekel, A. 2002, *ApJ*, 568, 52
- Wechsler, R. H., Zentner, A. R., Bullock, J. S., Kravtsov, A. V., & Allgood, B. 2006, *ApJ*, 652, 71
- Wetzel, A. R., Cohn, J. D., & White, M. 2008, *ArXiv e-prints*
- Zehavi, I., Weinberg, D. H., Zheng, Z., Berlind, A. A., Frieman, J. A., Scoccimarro, R., Sheth, R. K., Blanton, M. R., Tegmark, M., Mo, H. J., et al. 2004, *ApJ*, 608, 16
- Zhao, D. H., Jing, Y. P., Mo, H. J., & Boerner, G. 2008, *ArXiv e-prints*
- Zheng, Z. 2004, *ApJ*, 610, 61
- Zheng, Z., Berlind, A. A., Weinberg, D. H., Benson, A. J., Baugh, C. M., Cole, S., Davé, R., Frenk, C. S., Katz, N., & Lacey, C. G. 2005, *ApJ*, 633, 791
- Zheng, Z., Zehavi, I., Eisenstein, D. J., Weinberg, D. H., & Jing, Y. 2008, *ApJ*, submitted, arXiv:0809.1868 [astro-ph]